Ultrafast Dynamics of Isolated Phenylcarbenes Followed by Femtosecond Time-Resolved Velocity Map Imaging

Bastian Noller,[†,‡] Lionel Poisson,[†] Raman Maksimenka,[†] Oliver Gobert,[†] Ingo Fischer,[‡,*] and J. M. Mestdagh[†,*]

Laboratoire Francis Perrin, CNRS URA 2453, CEA IRAMIS/Service des Photons, Atoms et Molécules, F-91191 Gif-sur-Yvette Cedex, France and University of Würzburg, Institute of Physical Chemistry, Am Hubland, D-97074 Würzburg, Germany

Received: December 12, 2008; Revised Manuscript Received: January 21, 2009

The ultrafast dynamics of two carbene model systems, chlorophenylcarbene (CPC) and trifluoromethylphenylcarbene (TFPC), has been studied in a molecular beam. Velocity map imaging aids optimizing the pyrolysis conditions for a clean generation of reactive intermediates by supersonic jet flash pyrolysis. The dynamics was followed in real time by time-resolved mass spectroscopy and photoion and photoelectron imaging. CPC was excited at 265 nm into the $3\ ^1A'$ state, corresponding to excitation from a π-orbital of the aromatic ring into the lowest unoccupied molecular orbital, which contains the p-orbital at the carbene center. The experimental results suggest a three step deactivation process in agreement with computations. TFPC exhibits two absorption bands in the 36000 cm^{-1} and 41000 cm^{-1} range and gives rise to very similar dynamics, although it has a triplet ground state. The experimental data were augmented by computations.

Introduction

This paper presents a full account of our work on the spectroscopy and femtosecond dynamics of chlorophenylcarbene (CPC) and trifluoromethylphenylcarbene (TFPC) studied in a supersonic jet (Scheme 1). It follows a communication of preliminary results[1] and earlier papers on the ultrafast dynamics of radicals.[2,3]

Carbenes can be regarded as model systems for examining nonadiabatic coupling, because of the large density of low-lying electronically excited states. They have been described as "a test ground for electronic structure methods" in the literature.[4] In practice, arylcarbenes play key roles in rearrangements of alkylated aromatic compounds at high temperatures and might be important in industrial cracking processes.[5] Depositing a well-defined amount of energy into the molecule by laser excitation and following its photophysics in real time can help one to understand the nature of such rearrangements and physical processes initiating them. Note that possible thermal and photochemical isomerizations of arylcarbenes directly depend on the substituents of the aryl ring as well as the second substituent linked to the carbene center.[6]

Since experimental data on the photochemistry of phenylcarbenes are scarce, a detailed picture has not been achieved so far.[7,8] The photochemically induced isomerization of CPC to 1-chlorocyclohepta-1,2,4,6-tetraene (CCHT) has been studied by matrix isolation techniques.[9] Femtosecond time-resolved experiments in the liquid phase document the photolysis of diazirines and give insight into the photochemical formation of arylhalocarbenes.[10] But, so far, no information has been available on the primary photophysical processes of isolated arylcarbenes themselves. Primary photophysical processes such as internal conversion (IC), intersystem crossing (ISC), and relaxation through conical intersections (CIs) initiate almost all photoreactions, and photochemistry rarely takes place from the initially excited state.[11] The elucidation of such processes is thus of considerable importance for understanding phenylcarbene photochemistry.

SCHEME 1: Carbene Generation by Supersonic Jet Flash Pyrolysis of Diazirines

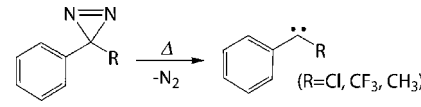

In our recent communication, we presented experimental results that support a deactivation of the initially excited-state in a three-step process to the hot ground state.[1] The present paper gives a full account of the early dynamics of CPC, together with new results on TFPC.

The phenylcarbenes were produced from diazirines, which are known to be ideal precursors for generating free carbenes[12] and are important compounds for photoaffinity labeling.[13] The diazirines were cleaved by supersonic jet flash pyrolysis to form a cold molecular beam of intermediates.[14] Diazirines with different functional groups were used, showing that not all of them are suitable for phenylcarbene generation by this method. Velocity map imaging (VMI)[15] has proven to be a powerful tool for studying intermediates in order to distinguish between pyrolytically generated intermediates and intermediates produced by dissociative photoionization of the precursor, an issue that is important for the interpretation of spectroscopic data.[16] The method thus greatly simplifies the optimization of the pyrolysis conditions and seems to be of general interest for efficiently studying reactive intermediates.

Resonance enhanced multiphoton ionization (REMPI) spectroscopy was applied to characterize the absorption spectrum of TFPC. The singlet−triplet gap of TFPC was determined by density functional theory (DFT) calculations. The dynamics of the two studied phenylcarbenes (CPC and TFPC) are interesting

* Corresponding author. E-mail: jean-michel.mestdagh@cea.fr; ingo@phys-chemie.uni-wuerzburg.de.
† CNRS URA 2453.
‡ University of Würzburg.

10.1021/jp810974m CCC: $40.75
Published on Web 02/26/2009

to compare, since they possess different spin multiplicity in the ground state as known from experimental as well as theoretical results. Whereas CPC has a singlet ground state,[17,18] ESR spectra show that TFPC has a triplet ground state, but to the best of our knowledge no computational information on the singlet−triplet gap is available yet.[19] Hence the present work explores and compares dynamics on singlet and triplet potential energy surfaces of structurally very similar molecules.

Experimental Section

The experiments were performed in a standard molecular beam apparatus. A cold beam of phenylcarbenes was prepared by supersonic flash pyrolysis[14] of diazirines (3-phenyl-3-(trifluoromethyl)diazirine, 3-phenyl-3-methyldiazirine (isomerized), and 3-phenyl-3-chlorodiazirine), synthesized according to the literature.[20−22] The precursor was seeded in 3 bar of argon and expanded through a short, weakly heated silicon carbide (SiC) tube attached to a water-cooled solenoid pulsed valve operating at 20 Hz. The cooling system assures a stable operation of the valve and suppresses the dissociation of the precursor before reaching the end of the SiC tube. The pressure in the source chamber was 2×10^{-5} mbar. After passing a 1-mm skimmer, the molecular beam reached the detection chamber (2×10^{-7} mbar), which was equipped with a time-of-flight mass spectrometer (TOF-MS) and a VMI detector used for mapping ion or electron kinetic energy distributions. Photoelectrons and ions were detected on a position-sensitive detector, creating raw images that were recorded for each delay and accumulated over several hundred laser shots. The images were then transformed by the pBASEX[23] method to reconstruct the central slice of the original kinetic energy distribution of the photoelectrons or ions from the raw images, yielding photoelectron or photoion spectra as a function of the time delay between the pump and probe laser. Also, the pBASEX algorithm enables the separation of polarized and unpolarized structures in the image.[15]

A 20 Hz femtosecond Ti:Sa oscillator/amplifier chain was used for the experiments. In accordance with the absorption spectrum of the carbenes, the third harmonic of the Ti:Sa laser (265 nm, 2 μJ) was used as a pump pulse. Following the initial excitation, the fundamental of the Ti:Sa (795 nm, 480 μJ) was applied as the probe pulse in a multiphoton ionization process.

Since the ionization potential (IP) of the carbene is low, and the excited states form a dense band between 3.9 and 6 eV, elucidating the primary photophysical processes of the 3 ^{1}A′ with a single probe photon is unlikely to give a sufficient pump−probe contrast, since the photons of pump (265 nm) and probe (e.g., 275 nm to reach the ionization threshold) will lie energetically too close. Using 795 nm photons for the probe step produced a very strong two color contrast. Nevertheless, due to the large density of excited states of arylcarbenes, applying a multiphoton probe can lead to photoelectron spectra which are mediated by intermediate resonances and can hamper the interpretation.[24−26]

Both laser beams were horizontally polarized. The pump−probe time delay was controlled by means of a delay line set on the probe beam and actuated by a computer-controlled stepper motor. The time intervals between two data points were not constant in a given time scan and adjusted to the slope of the decay signal. Around zero time delay, data points were taken typically every 8 fs, whereas, at early and late delay times, longer intervals were chosen. The beams were overlapped in a small angle and focused into the interaction region by a 70 cm lens for the 265 nm beam and a 50 cm lens for the 795 nm one.

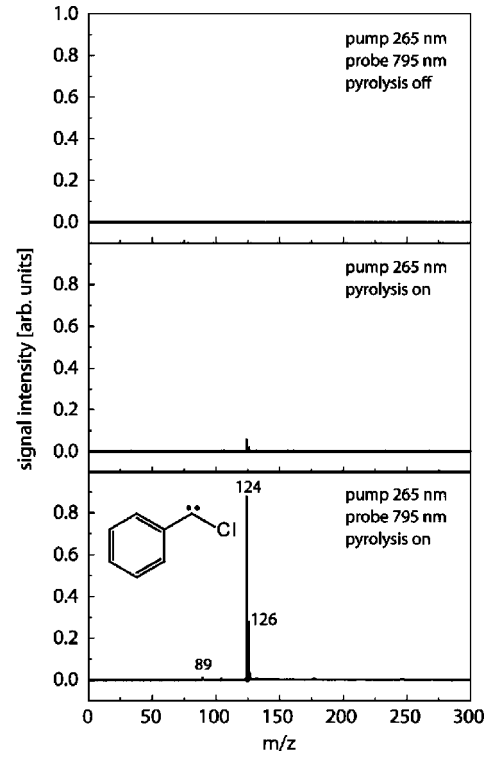

Figure 1. Mass spectra of 3-phenyl-3-chlorodiazirine recorded at zero time delay at different conditions. When turning the pyrolysis on, the carbene signal (m/z = 124/126) increases strongly (bottom trace). In two-color experiments, a strong pump−probe contrast is achieved.

The 795 nm beam was focused 5 cm away from the interaction region; the focus for the 265 nm beam was 14 cm away. For pump−probe contrast optimization, the probe and the pump beam were attenuated until the one-color background signal was minimized. The laser cross-correlation of pump and probe was typically around 100 fs. Good starting values for zero time delay as well as the instrument response function (IRF) were taken from experiments on C_7H_5 (compare Figure 6). In the time-delay scans, 256 shots were averaged per data point. The time-resolved spectra reported here typically constitute an average of four to five such scans.

Frequency resolved spectra of TFPC and styrene were acquired in a separate standard molecular beam apparatus,[27] equipped with a TOF-MS. For excitation, the unfocused frequency-doubled output of a tuneable nanosecond dye laser was used (beam diameter around 0.35 cm), which was pumped by the third harmonic of a Nd:YAG laser. The carbens were produced in the same manner as described above, and the measurements were performed using one-color REMPI spectroscopy.

Experimental Results

Carbene Generation. The pyrolytic generation of the phenylcarbenes is illustrated in Scheme 1. The precursors corresponding to R = Cl and R = CF_3 show full conversion to the carbene, already at low pyrolysis temperature. Only a small amount of one-color background and negligible quantity of side products are observed in the mass spectrum as shown in Figure 1. In contrast, we discuss below that this approach is unsuccessful when R = CH_3. Typical TOF mass spectra obtained in the femtosecond experiments on 3-phenyl-3-chlorodiazirine (R = Cl) are depicted in Figure 1 at different conditions.

The spectrum in the upper trace has been recorded with the pyrolysis source turned off and both excitation (265 nm) and

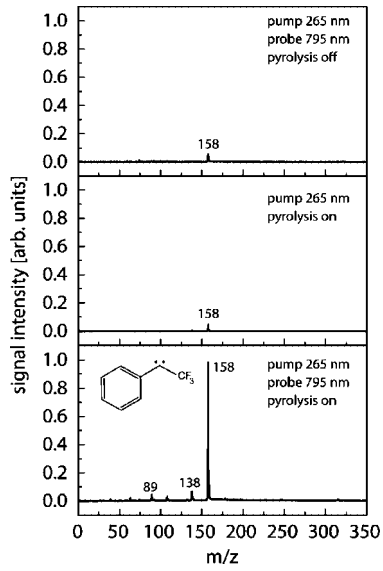

Figure 2. Mass spectra of 3-phenyl-3-trifluoromethyldiazirine recorded at zero time delay at different conditions. When turning the pyrolysis on, the carbene signal ($m/z = 158$) increases strongly (bottom trace). With two colors, a pronounced pump−probe contrast is achieved.

probe (795 nm) laser arriving at around zero time delay. Only when strongly zooming into the mass spectrum (not shown) a negligible signal at the mass of the carbene ($m/z = 124$) was visible under these conditions, due to dissociative photoionization of the precursor. The amount depends on the position in the molecular beam pulse (i.e., at the leading edge of the pulse, only pyrolytically generated carbenes are present and no carbenes resulting from dissociative photoionization of the precursor). This observation is in accord with recent studies on the dissociative photoionization of diazirines using synchrotron radiation.[28] When turning the pyrolysis on, the carbene signal increases by a factor of 100−1000 (bottom trace), depending on the position in the molecular beam. CPC shows the typical chlorine isotopic distribution ($^{35}Cl/^{37}Cl$: 76%/24%) as well as ^{13}C satellites. The center trace is recorded with the probe laser alone. A comparison of the center and bottom traces illustrates the pronounced pump−probe contrast of the CPC signal. Note that, for the delay scans, the pump laser was attenuated to produce a very tiny one-color signal, whereas the probe laser was adjusted to give no one-color signal at all. The second product of the pyrolysis is N_2, which is neither excited nor ionized at the chosen wavelengths. Experiments using the second harmonic of the Ti:Sa laser (398 nm) as probe wavelength did not result in a sufficient pump−probe contrast. A very small signal is also present at $m/z = 89$. The time dependence of this mass signal, corresponding to C_7H_5, is different from the time dependence of CPC as will be discussed below.

The mass spectra of 3-phenyl-3-(trifluoromethyl)diazirine ($R = CF_3$) are presented in Figure 2. Again the diazirine is cleaved efficiently at low pyrolysis temperatures. Similarly clean spectra were also obtained using the nanosecond setup for the REMPI experiments as well as for control experiments with 118 nm VUV light (not depicted). When turning the pyrolysis on, the carbene signal ($m/z = 158$) increases by a factor of 10. When adding the probe laser, a significant pump−probe contrast is achieved as visible in the bottom trace of Figure 2. For the pump−probe experiments the laser power of the 795 nm probe was attenuated to give no one-color signal in the TOF-MS. The fragments with $m/z = 138$ and $m/z = 89$ correspond to the loss of HF and CF_3, respectively. Both masses show the same time

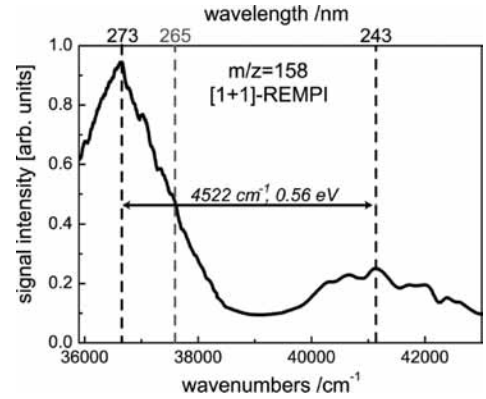

Figure 3. REMPI spectrum of TFPC, recorded using a nanosecond dye laser.

dependence and thus originate from dissociative photoionization, which is discussed in more detail below (Figure 7). This fragmentation pattern is presumably linked to the multiphoton probe step and was not observed in one-color VUV experiments when applying synchrotron radiation up to 9.5 eV.[28]

A [1 + 1]-REMPI spectrum was recorded for TFPC using the nanosecond dye laser setup. It is presented in Figure 3. The spectrum shows two broad and unstructured bands. The first band is peaked at 36650 cm^{-1}, and a second weaker band is peaked at around 41140 cm^{-1}. The spectrum shows that TFPC absorbs at 265 nm, allowing femtosecond pump−probe experiments using the Ti:Sa third harmonic for excitation of the intermediates. For CPC, all attempts to record a [1 + 1]-REMPI spectrum using the nanosecond dye laser setup failed.

The recorded REMPI spectrum of TFPC is similar to the UV/vis spectrum recorded in matrix experiments[29] of a closely related phenylcarbene, TFPC-COOH, which was produced by irradiation of 4-(1-azi-2,2,2-trifluoroethyl)benzoic acid (ATEBA). The two carbenes only differ in the presence of a COOH group at the aryl ring. No UV/visible (UV/vis) absorption spectrum of TFPC is available in the literature. A strong absorption around 36000 cm^{-1} seems to be characteristic for TFPC entities, since the UV/vis absorption spectrum obtained after irradiation of ATEBA in ethanol[29] shows an intense band at 35714 cm^{-1}. This band of the corresponding carbene (TFPC-COOH) is red-shifted compared to TFPC, due to the presence of a −COOH group. The weaker band of TFPC appearing at 41136 cm^{-1} in the REMPI spectrum is not visible in the UV/vis spectrum of TFPC-COOH reported in the literature, since it is superposed by a much stronger absorption band of the remaining ATEBA precursor in this spectral region.

As a second detection method, photoion imaging was applied. In contrast to conventional TOF mass spectrometry, this mass selective method registers not only the different ion masses, but also the position at which they collide with the detector. Thus particles with higher kinetic energy will hit the detector on a bigger radius. By processing the raw images via the pBASEX algorithm, the kinetic energy distribution of the particles is accessible. Typical photoion images of 3-phenyl-3-chlorodiazirine, which was irradiated by 265 nm only (150 μJ) are depicted in Figure 4. Note that these images were recorded later in the molecular beam as compared to the TOF spectra in Figure 1, and the laser power at 265 nm was considerably higher as in the pump−probe experiments. Later in the molecular beam, the concentration of diazirines is higher, whereas the maximum concentration of pyrolytically generated intermediates is found at the leading edge of the gas pulse. When the pyrolysis is turned off, the 3-phenyl-3-chlorodiazirine yields

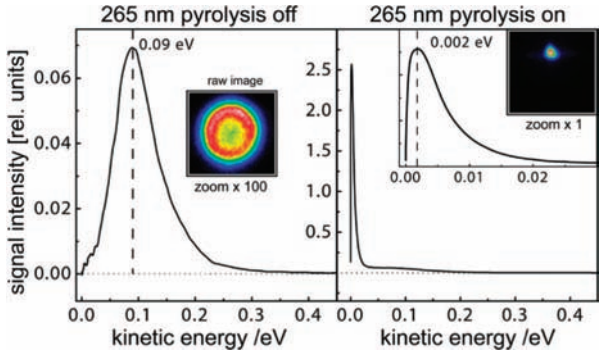

Figure 4. Kinetic energy distributions of the carbene ions (mass m/z =124) with pyrolysis source off (left) and on (right) recorded by VMI. The raw images are depicted as insets. The intensity of the signal strongly increases when turning the pyrolysis on, and the kinetic energy distribution becomes very narrow (note the same x-axis scale). The kinetic energy distribution with pyrolysis on between 0.00 and 0.03 eV is magnified as an inset on the right-hand side.

a ring of fragments at the mass of the CPC (m/z = 124, left) in the images. The corresponding kinetic energy distribution of these fragments is peaked at 90 meV. Their energy distribution and the corresponding raw image (inset) are presented in Figure 4.

Comparison with recent synchrotron experiments proves that the fragments are formed by dissociative photoionization of the precursor by two 265 nm photons.[28] The VUV synchrotron measurements show that dissociative photoionization of CPC-N_2 takes place above 8.8 ± 0.1 eV. Because of the excess energy (0.56 eV) deposited into the precursor, it dissociates after ionization into nitrogen and CPC^+ with considerable kinetic energy. When turning the pyrolysis on, the ring continuously fades out, and an intense spot appears at the same mass (m/z = 124, CPC), which has a higher velocity in the direction of the molecular beam (Figure 4, right) and a very narrow kinetic energy spread with its maximum peaked at 2 meV.

A magnified plot of the narrow energy distribution is shown as an inset in the right-hand side of Figure 4. These ions are no longer produced by dissociative photoionization of the precursor in the ionization region but by a [1 + 1]-REMPI process of pyrolytically generated carbenes in the beam. Thus by monitoring the speed distribution of the ions as a function of the pyrolysis temperature, the conditions of intermediate generation can easily be optimized. The method allows distinguishing between carbenes originating from the pyrolysis source (spot) and carbenes formed by dissociative photoionization (or photodissociation) of the precursor (ring). This simplifies the interpretation of spectroscopic data, since dissociative photoionization or photodissociation processes leading to fragments can safely be discriminated from intermediates originating from the pyrolysis source. Similar observations were made when using 3-phenyl-3-(trifluoromethyl)diazirine. Hence we were able to optimize the generation of TFPC in the same way.

REMPI spectroscopy was performed to experimentally determine the absorption spectrum of the product obtained by supersonic jet flash pyrolysis of 3,3-methylphenyldiazirine. The result is presented below in Figure 5 and compared to the spectrum obtained when using authentic styrene (mass spectra are presented in the Supporting Information). Between 35 600 cm^{-1} and 36 000 cm^{-1}, the REMPI spectrum of styrene shows the same structure that was also acquired by fluorescence spectroscopy, and our spectrum augments it up to 37 200 cm^{-1}.[30] The experiment shows that styrene has a major contribution in the molecular beam. Hence a barrier of only 31 kJ/mol is not

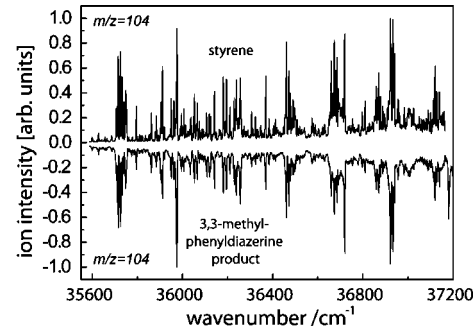

Figure 5. [1 + 1]-REMPI spectrum of authentic styrene compared to the pyrolysis product of 3,3-methylphenylcarbene. 3,3-methylphenyldiazirine produces styrene in high concentrations.

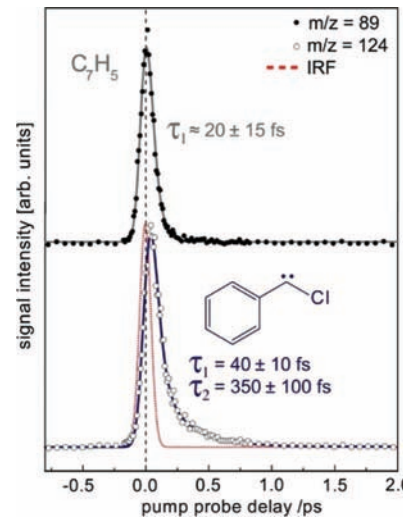

Figure 6. Ion signal of CPC (R=Cl, lower trace) and the C_7H_5 isomer (top trace) as a function of the time delay (pump 265 nm, probe 795 nm). The signal is described by a two step decay for CPC, whereas the C_7H_5 can be described by a monoexponential decay. The IRF is presented as a dotted red line.

sufficient to generate a clean beam of methylphenylcarbene (MPC, compare computational section). This control experiment also proves that we are able to produce a vibrationally cold molecular beam using supersonic jet flash pyrolysis of diazirines. Experiments using deuterated 3,3-methylphenyldiazirine (R = CD_3) showed no conclusive evidence of deuterated MPC in the beam (see Supporting Information), which is known to have a higher barrier toward isomerization,[31] due to a reduced possibility of tunneling.

Time-Resolved Measurements. Three different experimental techniques were used to elucidate the excited-state dynamics of the phenylcarbenes: (a) measurements of the time-dependent ion signal by a standard TOF-MS, (b) time-resolved ion imaging, and (c) time-resolved photoelectron imaging. After optimization of the pyrolysis source, experiments (a) and (b) yielded identical results. Typical mass selected delay scans obtained for CPC and TFPC are depicted in Figure 6 and Figure 7, respectively (both lower trace). The carbene signals are compared with delay curves of other fragments present in small quantities in the mass spectra (upper traces). The ion signal of both carbenes is described by a two-step decay, convoluted by a Gaussian shaped IRF for both carbenes (full width at half-maximum (fwhm) = 105 fs for CPC, 95 fs for TFPC). The IRF was optimized in a global fitting procedure of the dynamic models of both delay scans shown in Figure 6. The zero time delay and the fwhm of the laser cross correlation was shared in the global fit. The model

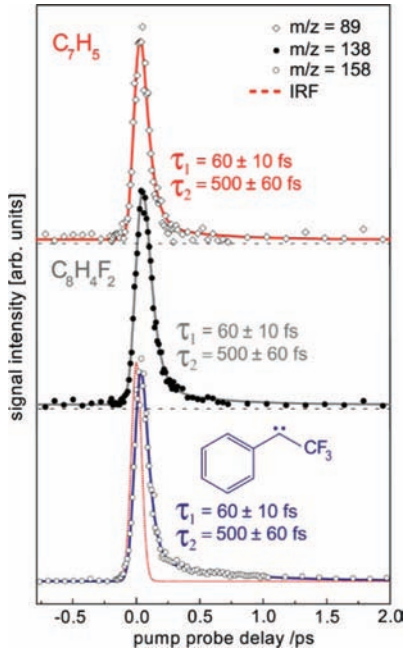

Figure 7. Ion signal of TFPC (R = CF_3, bottom trace), the $C_8H_4F_2$ isomer (middle trace), and the C_7H_5 isomer (top trace) as a function of the time delay (pump 265 nm, probe 795 nm). The signal is well described for all species by using the same model and equal time constants.

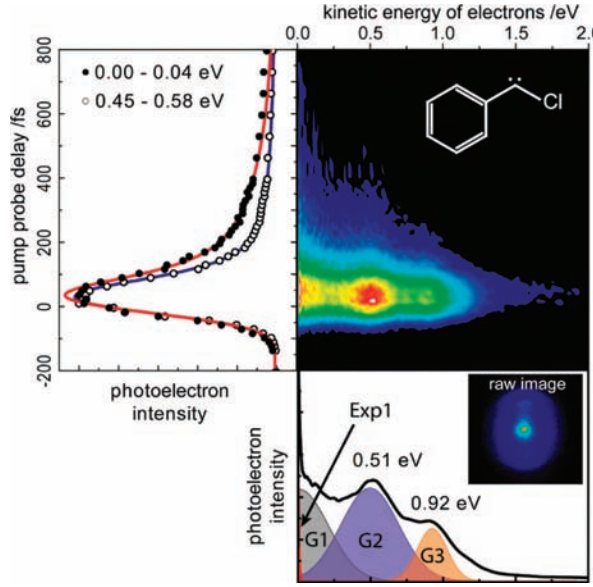

Figure 8. TRPES of CPC (pump 265 nm probe 795 nm). The photoelectron spectrum shows the unpolarized part of the images. Photoelectrons with low kinetic energy do not fully decay to zero after 1 ps (left). The averaged photoelectron spectrum shows three bands (bottom).

for CPC reflects a two step deactivation process between three transients (I → II → III).[32] Both signals apparently decay to zero at long time, suggesting that transient III is not efficiently ionizable in the probe step with 795 nm photons. Hence the experimental time-resolved ion signal was described by a linear combination of $S^{I}_{(\Delta t)}$ and $S^{II}_{(\Delta t)}$ shown in equations 1 and 2. $S^{I}_{(\Delta t)}$ describes the monoexponential decay of state I with a time constant of τ_1, and $S^{II}_{(\Delta t)}$ describes the monoexponential rise (τ_1) and monoexponential decay (τ_2) of state II.[32] The parameter σ is proportional to the fwhm of the IRF (fwhm = 2.356 × σ).

$$S^{I}_{(\Delta t)} = \exp\left[\frac{1}{2\tau_1}\left(\frac{\sigma^2}{\tau_1} - 2\Delta t\right)\right]\left[1 + \mathrm{Erf}\left(\frac{\Delta t - \frac{\sigma^2}{\tau_1}}{\sqrt{2}\sigma}\right)\right] \quad (1)$$

$$S^{II}_{(\Delta t)} = \exp\left[\frac{1}{2\tau_2}\left(\frac{\sigma^2}{\tau_2} - 2\Delta t\right)\right]\left[1 + \mathrm{Erf}\left(\frac{\Delta t - \frac{\sigma^2}{\tau_2}}{\sqrt{2}\sigma}\right)\right] - \exp\left[\frac{1}{2\tau_1}\left(\frac{\sigma^2}{\tau_1} - 2\Delta t\right)\right]\left[1 + \mathrm{Erf}\left(\frac{\Delta t - \frac{\sigma^2}{\tau_1}}{\sqrt{2}\sigma}\right)\right] \quad (2)$$

As documented in our preliminary communication, a description of the time-dependent ion signal of CPC by a monoexponential decay curve (I → II, $S^{I}_{(\Delta t)}$) is not adequate.[1] At this point, our results show that both carbenes have an ultrafast initial relaxation process on the order of τ_1 = 30−70 fs, followed by a second relaxation process, which is about 10 times slower. However, as will be described below, two time constants are not sufficient to describe the dynamics of CPC.

When recording the time-resolved spectra for CPC, a small mass peak was present at m/z = 89 (C_7H_5). Its time dependence is presented in the top trace of Figure 6 and differs strongly from the signal of CPC. The time dependence is adequately described by a single exponential convoluted with the IRF (state I to state II model, $S^{I}_{(\Delta t)}$). The state lifetime was measured to lie around 20 fs. Due to the difference in dynamics, we believe that this species is formed from CPC during pyrolysis by an irreversible loss of Cl and not due to dissociative photoionization from the parent. It might correspond to phenylcarbyne, which is formed upon C−Cl bond cleavage in CPC. However, several minima on the ground-state potential energy surface of C_7H_5 are known in the literature from quantum chemical calculations.[33] It is thus not clear which of these isomers is generated in the pyrolysis. Because of the small signal size, it is not considered in the discussion of the photoelectron spectra.

In contrast to CPC, the small mass peaks observed at m/z = 89 and m/z = 138 while studying TFPC (Figure 2) show the exact same time dependent signal as was found for TFPC and correspond to the loss of CF_3 and HF, respectively (Figure 7). These fragments are likely to result from dissociative photoionization of the parent $TFPC^+$ in the probe step.

A deeper insight into the excited-state dynamics of polyatomic molecules was obtained by time-resolved photoelectron spectroscopy (TRPES).[11] The time-resolved photoelectron spectra, extracted from velocity map electron imaging, of CPC and TFPC are depicted in Figure 8 and Figure 10, respectively. The images show a contour plot of the photoelectron intensity as a function of kinetic energy (horizontal axis) and time delay (vertical axis). The bottom PES in Figure 8 consists of an average over all delay times, showing diffuse broadened structures in the electron spectra. The spectra of CPC and TFPC are rather similar in appearance and can be described by a superposition of three Gaussian functions (G1, G2, G3) and one exponential function for electrons with very low kinetic energy. This choice of describing the photoelectron spectrum does not intend to reflect a possible mechanism. It was chosen for convenience in order to assign reliable time constants to different electron energy envelopes. The spectrum of CPC shows one very sharp peak around zero kinetic energy (0.00−0.04 eV, EXP1), one broadband extending from 0.00−0.25 eV (G1), one very broad

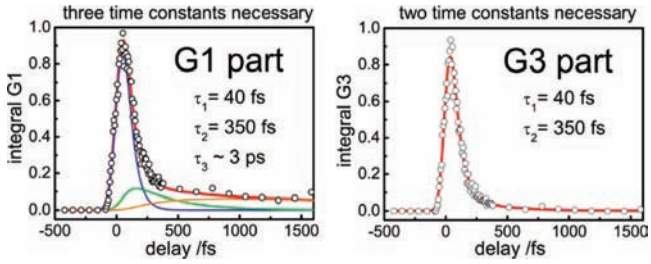

Figure 9. Time dependent integrals of the functions G3 and G1 of CPC. Both integral functions were normalized to the maximum intensity for ease of comparison. G3 decays to zero, whereas, for G1, a third time constant is necessary in order to describe the time evolution.

unstructured band around 0.51 eV (0.45−0.58 eV, G2), and a third broad band at 0.92 eV (G3).

The two broad bands to the right (0.51 and 0.92 eV) in the PES yield the same time dependence as the mass resolved ion signal presented in the lower trace of Figure 6. They can be described by two overlapping Gaussians G2 and G3 (Figure 8, bottom). These two bands show the largest contribution to the intensity of the photoelectron spectra. On the left-hand side of Figure 8, the time-dependent photoelectron signal of electrons with low kinetic energy (0.00−0.04 eV) is compared to the signal originating from photoelectrons between 0.45 and 0.58 eV. The decay curves were normalized to the same maximum signal intensity, and differences at long delay times are apparent. In contrast to the high energy electrons, the signal of the photoelectrons with low kinetic energy is not well described by a fit with only two time constants. This part of the signal was additionally described as the superposition of an exponential decay function (Exp1) and a broad Gaussian function centered at 0 eV (G1). Note that the contribution of Exp1 is small compared to G1. When performing a least-squares fit of the linear combination (Exp1+G1+G2+G3) while optimizing the amplitudes of each function, the spectra can be adequately described at all delay times. The integral of each of the four functions was then determined as a function of the time delay between pump and probe. In all recorded spectra the G1 integral (as well as the Exp1 integral) did not decay to zero in the recorded time period, as can be seen on the left-hand side of Figure 9, in which the time dependence of the G1 integral is compared to the time dependence of the G3 integral. The time-dependent integrals of G2 and G3 yield the same time dependence as the mass peak of CPC (compare Figure 6). Thus, only the dynamics of G1 (and Exp1) shows significant deviations. The time dependent signal is no longer well described by a two step deactivation scheme. A model transient I → transient II → transient III → transient IV is required in order to properly describe the dynamics of G1 (Figure 9). A third time constant in the order of 3 ps appears when plotting the integral of G1 (or Exp1) as a function of the delay time.

The electron images also carry information on the angular distribution of the electrons. The pBASEX algorithm used for analysis of the photoelectron images also analyzes the angular distribution and can distinguish polarized (P_2) and unpolarized (P_0) parts of the photoelectron images.[15] Figure 8 and Figure 10 depict only the time evolution of the isotropic P_0-part of the images, which holds a much higher contribution to the overall electron signal. The P_2-part, which is not shown here, has significant contributions for electrons with a nonzero kinetic energy only. The Exp1 and G1 function are no longer required in the description of the PES for the polarized (P_2) part of the photoelectron images. This indicates that the low kinetic energy

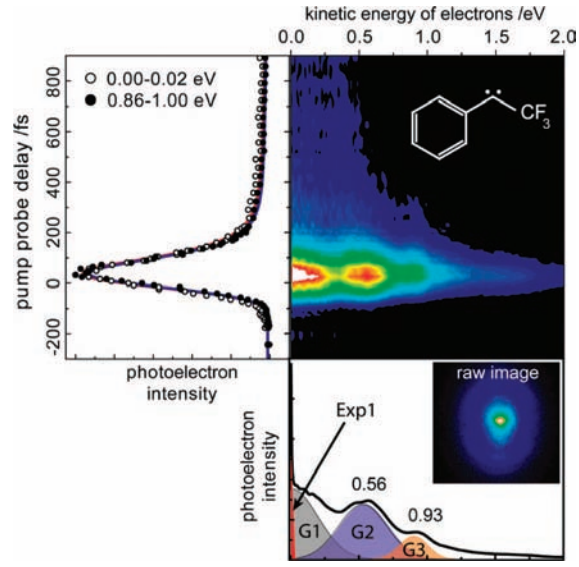

Figure 10. TRPES of TFPC (pump 265 nm probe 795 nm). The photoelectron spectrum shows the P0 part of the images. Photoelectrons with low kinetic energy do not fully decay to zero after 1 ps (left). The averaged photoelectron spectrum shows one sharp peak and three bands (bottom).

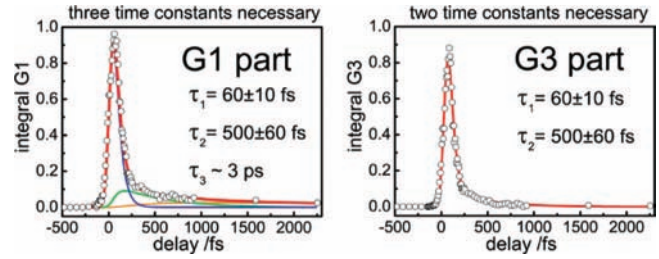

Figure 11. Time dependent integrals of the functions G3 and G1 of TFPC. Both integral functions were normalized to the maximum intensity for ease of comparison. G3 decays to zero, whereas, for G1, a third time constant is necessary in order to describe the time evolution.

electrons (Exp1+G1) originate from autoionization processes. In contrast, the polarized P_2-contribution to electrons above 0.25 eV suggests that such electrons originate from a direct ionization process.

The time-dependent photoelectron spectra of TFPC can be analyzed in the same manner as was done for CPC. The spectra are rather similar in appearance and only differ in the positions of G2 and G3 as well as in the magnitude of the time constants. The G3 part is well described by two time constants ($\tau_1 = 60$ fs, $\tau_2 = 500$ fs), whereas for the G1 part again an additional time constant is required ($\tau_3 \sim 3$ ps) (see Figure 11). The time dependent ion signal of TFPC depicted in the lower trace of Figure 7, revealed only two time constants ($\tau_1 = 60$ fs, $\tau_2 = 500$ fs). The same time constants are also found in the G3 part of the TRPES.

Computations

Methods and Procedures. Depending on the functional groups, some phenylcarbenes are known to perform a ring expansion to cycloheptatetraenes (CHTs). Hence the C-shift reaction coordinate was scanned in a DFT calculation using the BMK/6-311^{+2}G** level of theory (compare Scheme 2 and Figure 12) to validate that no isomerization takes place in the pyrolysis nozzle. A preliminary account of this appeared in a recent communication,[1] which is now presented extensively.

SCHEME 2: C-Shift of CPC to CCHT with Illustration of the Scanned Coordinate

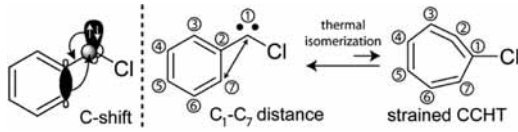

For the theoretical study, the BMK functional, explicitly developed for modeling thermochemical kinetics, was chosen.[34] It was used as implemented in the Gaussian 03 set of programs.[35] The distance between C_1-C_7 is considerably smaller in CCHT than in CPC (compare Scheme 2). Hence, for a first good approximation, a relaxed potential energy surface scan was performed along this coordinate as suggested in ref 36 for the ring expansion. The geometry at the maximum potential energy of the scan was used as a guess for the transition state of the isomerization and was subsequently used in a QST3 calculation[37] for further improvement. The transition state, the reactant (CPC), as well as the product (CCHT) were optimized separately with tight convergence criteria, and the electronic energies were zero point energy corrected (ZPEC).

For CPC, extensive *ab initio* and DFT calculations on the singlet−triplet gap have been performed by the Platz group,[18] demonstrating that the B3LYP functional is a cost-effective method to compute this important parameter.[38] No calculations exist on the singlet−triplet gap of TFPC, even though experimental evidence concludes that it has a triplet ground state.[19] In order to acquire a value for the gap of TFPC a full optimization with the UB3LYP/6-311^{++}G**, UBLYP/6-311^{++}G**, BVWN5/6-311^{++}G**, and BVWN5/6-311^{++}G-(2df,2p) functional/basis sets was carried out for the singlet as well as for the triplet carbene. The sum of electronic and ZPE was compared for each method (Table 1). The UBLYP and BVWN5 functionals were used, because they were found to yield good values for the singlet−triplet gaps of other carbenes.[39]

To acquire an approximation of the first excited-state energy of the CPC^+ ion (vertical geometry), TD-B3P86/6−311^{++}G** calculations were performed using the ground-state equilibrium geometry. The ground-state equilibrium geometry was taken from the B3LYP calculations of CPC.

Computational Results. As visible in Table 1, all DFT calculations yield a triplet ground-state for TFPC, regardless of the functional employed. According to the UB3LYP/6-311^{++}G** calculations, the first singlet state is located approximately 17.4 kJ/mol higher in energy at B3LYP level of theory. In comparison, the same level of theory gave a singlet−triplet gap of −23.5 kJ/mol for CPC, which predicts the CPC correctly as a singlet in its ground-state and closely reproduces the benchmark result obtained in ref 18, The result for the TFPC fits nicely into a series of calculations performed on carbenes with different electronegative substituents reported in ref 40.

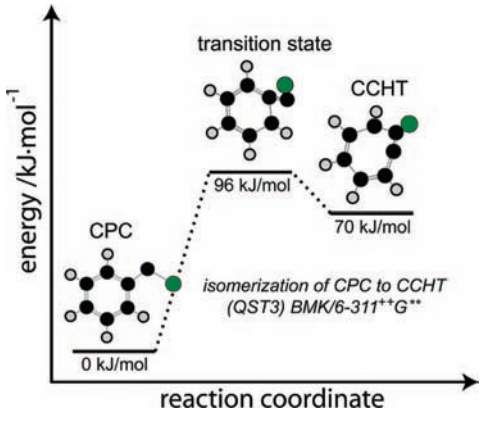

Figure 12. Energy diagram of the ground-state isomerization of CPC. The barrier was calculated using the BMK functional with 6-311^{+2}G** basis set. The transition state was found applying the QST3 method along the C−C distance coordinate. The energy corresponds to the sum of zero point and electronic energy.

TABLE 1: Overview of Calculated Singlet-Triplet Gaps[a]

method	TFPC [kJ/mol]	CPC [kJ/mol]
UBLYP/6−311^{++}G**	+10.8	
BVWN5/6−311^{++}G**	+13.8	
BVWN5/6−311^{++}G(2df,2p)	+15.9	
UB3LYP/6−311^{++}G**	+17.4	−23.5
UCCSD(T)/6−311G(2df,p) + ZPE (UB3LYP/6−31G*)		[−27.7][18]

[a] The value in brackets is taken from the literature.

The TD-B3P86/6-311^{++}G** method predicts the first excited-state of the CPC^+ ion at around 1.7 eV above the vertical ionization (same geometry as CPC in the ground state) potential of CPC. For the adiabatic case (geometry of the ground-state cation), the method yields a value of 1.9 eV.

In Figure 12 the results of the BMK calculations for the isomerization of CPC to CCHT are summarized. The ordinate represents the sum of electronic and zero point energy, and the abscissa represents the reaction coordinate of the isomerization to CCHT as illustrated in Scheme 2. The sum of electronic and zero point energy of CPC was arbitrarily defined as 0 kJ/mol as reference. The QST3 calculation[37] predicts an isomerization barrier for CPC to CCHT of 96 kJ/mol. The reverse barrier lies at only 26 kJ/mol and the carbene CPC is situated 70 kJ/mol lower in energy than CCHT.[1] The $\Delta_R G_m^0$ value for the CPC to CCHT reaction was calculated to lie at 69.1 kJ/mol.

In order to see how low a barrier can be before supersonic jet flash pyrolysis no longer generates the desired product out of the diazirine, 3,3-phenylmethyldiazirine (R = CH_3) was employed, which in principle should yield MPC. MPC is known to have only a very small barrier toward isomerization[31] to thermodynamically considerably more stable styrene via a [1,2]-H-shift. BMK/6-311G** (QST3) calculations employing the same procedure as described above for CPC, predict the barrier to lie at only 31 kJ/mol (Figure 13). The relaxed potential energy surface scan was performed along the C−C−H angle. The value for the isomerization barrier is close to the value retrieved by the BPW91/cc-pVDZ level of theory (23 kJ/mol) reported in the literature.[41]

Discussion

Carbene Generation. Producing a clean molecular beam of intermediates is associated with a considerable experimental challenge.[42] VMI[15] simplifies the discrimination between fragments formed by the source and fragments originating from dissociative photoionization or photodissociation by laser light as shown in Figure 4. Pyrolytically generated intermediates show a higher velocity along the expansion of the molecular beam and a very narrow velocity spread. Further VMI experiments on iodoalkanes showed that this approach is generally applicable also for other precursors. In the case of diazirines, the pyrolysis conditions could easily be optimized by following the images in real time. The diazirines cleave via dissociative photoion-

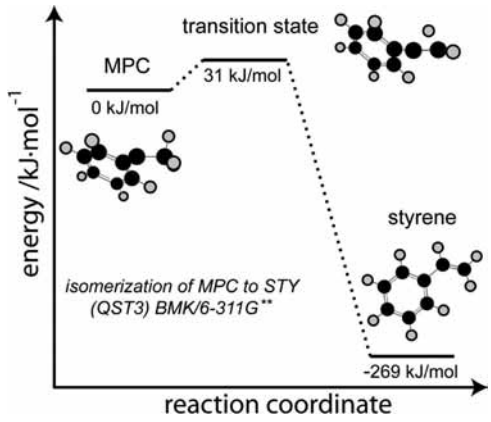

Figure 13. Energy diagram of the ground-state isomerization of MPC (singlet potential energy surface). The barrier was calculated using the BMK functional with 6−311G** basis set. The transition state was found applying the QST3 method along the C−C−H angle coordinate. The energy corresponds to the sum of zero point and electronic energy.

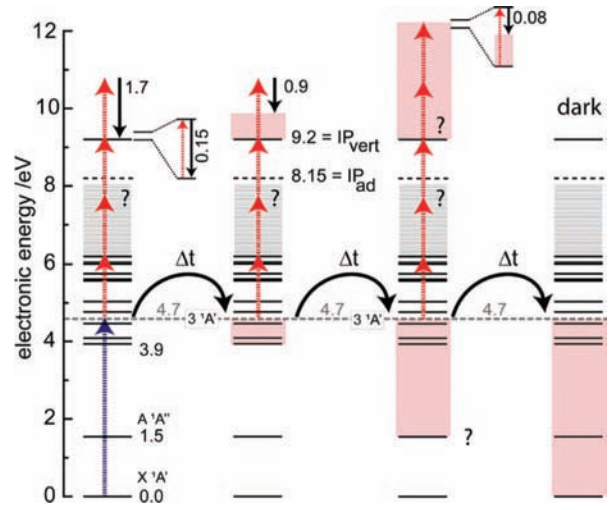

Figure 14. Excited states of CPC taken from ref 1. Most likely the initial excitation takes place into the 3 A′ state which holds by far the largest oscillator strength.

ization when irradiated, in agreement with recent synchrotron studies.[28] With 265 nm laser light, the CPC^+ fragments carry away 0.09 eV of kinetic energy. As visible in Figure 4, the images are not polarized, which indicates that the diazirines do not directly dissociate. We assume that dissociation occurs after more than a rotational period of the diazirine$^+$.

Because of the high reactivity of the carbenes, the possibility of isomerizations inside the pyrolysis has to be excluded. We emphasize that the thermodynamic stability of phenylcarbenes, with regard to isomerization, strongly depends on functional groups of the phenyl ring[6] as well as on the second substituent in α position to the carbene center. While flash vacuum thermolysis of phenyldiazirine (R = H) can produce CHT thermally,[8,43] depending on the trapping method, TFPC (R = CF_3) is known to be inert toward isomerizations.[13] Note that the technique of jet flash pyrolysis, applied in this study, achieves much shorter contact times, faster cooling, and can be optimized in real time while monitoring the pyrolysis products in the TOF-MS in contrast to earlier studies using vacuum thermolysis of diazirines. The second phenylcarbene (CPC, R = Cl) is known to be stable in condensed phase at room temperature.[17] The CPC is stabilized mesomerically by the free electron pairs of the chlorine atom.[36]

Our BMK calculations predict the carbene CPC to be 70 kJ/mol lower in energy than CCHT.[1] Thus CPC will be strongly favored on thermodynamical grounds. According to $\Delta_R G_m^0 = 69.1$ kJ/mol $= -RT \ln K$ and a pyrolysis temperature of approximately 800 K, the ratio of CPC/CCHT will be at around 40 000. In contrast to the equilibrium between CHT and phenylmethylene reported in ref 8, the chlorine atom considerably stabilizes the carbene, rendering it thermodynamically favored over CCHT. Hence we conclude that neither TFPC nor CPC isomerized during the pyrolytic generation from the corresponding diazirine precursors shown in Scheme 1. In contrast barriers of only 31 kJ/mol are not sufficient and MPC isomerizes to styrene when generated pyrolytically from the corresponding precursor.

Excited State Dynamics of CPC. In the case of CPC, *ab initio* calculations of the excited states are available[18] and are well reproduced by time-dependent DFT (TDDFT) calculations.[1] The TD-B3P86/6-311^{+2}G** energies of the excited states are depicted in Figure 14. All available calculations predict a relatively large energy gap between the A ^{1}A″ state and the next upper excited state. A dense assembly of electronic exited states exists between 3.9 and 6 eV, which are likely strongly coupled. This makes precise *ab initio* and TDDFT calculations challenging, since many electronic configurations contribute to the description of the electronically excited states in this energy region.[18] Taking the CASPT2 values for the location of the excited states from Platz et al.[18] instead of TDDFT values does not significantly changes the picture. When using the CASPT2 values, the A ^{1}A″ level rises by 0.2 eV and thus would predict electrons with 0.2 eV kinetic energy for detecting this state. Because of the broad bands in the experimental TRPES it is not clear whether TDDFT or CASPT2 gives the best description on the location of the excited states.

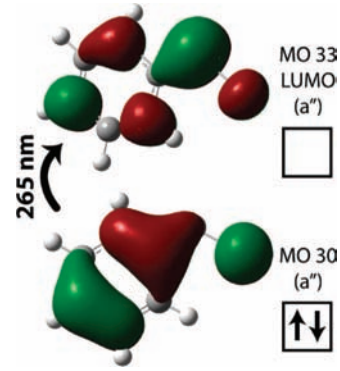

Figure 15. The excitation with the largest oscillator strength around 265 nm corresponds to a transition of an electron from orbital 30 into the LUMO of the molecule (MO 33). MO 33 holds a large coefficient at the carbene C-Atom.

In all calculations reported in the literature, the transition that carries the by far strongest oscillator strength in the energy region of 4.7 eV (265 nm) corresponds to the excitation of an electron from a π-orbital of the phenyl ring into the lowest unoccupied molecular orbital (LUMO) of the molecule (state 3 ^{1}A′) as illustrated in Figure 15. The LUMO contains a considerable contribution of the p-orbital at the carbene center, which is conjugated into the aromatic ring. The excitation energy is very sensitive to the details of the excited-state calculation. According to ref 18, it varies between 4.01 eV (309 nm) and 5.85 eV (212 nm). Hence a photon energy of 4.7 eV (265 nm) can be used for exciting the molecule.

The femtosecond time-resolved pump−probe experiments revealed that the initially excited-state of the phenylcarbenes

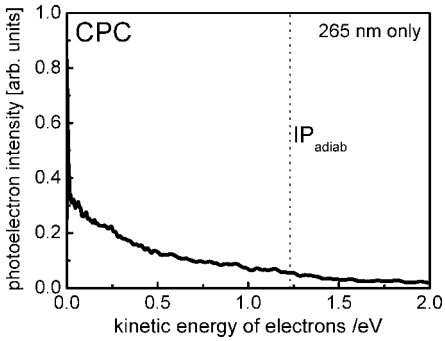

Figure 16. One-color PES recorded by VMI with 265 nm only. No structures are visible.

deactivates in a multi step fashion.[1] When analyzing the TRPES of CPC (Figure 8), most of the photoelectrons possess a kinetic energy of around 0.50 eV (open circles, left side) and a second broad peak is visible at around 0.91 eV. Both of the peaks show the same time dependence as the mass selected delay curve of Figure 6. Thus they are likely to correspond to the same photophysical processes. Since the dense manifold of excited states depicted in Figure 14 is not expected to result in well-separated bands in the TRPES, we assume that these broad bands result from ionization out of these states. The structure of the PES (G2 and G3) is not visible when static one-color photoelectron spectra are taken at higher laser intensities in with 265 nm only ([1 + 1] REMPI) as shown in Figure 16.

In this one-color spectrum, the band has its maximum at 0.05 eV and slowly falls off toward 1.25 eV in accord with the adiabatic and vertical IP measured in ref 28 (compare Figure 14), showing that Franck−Condon (FC) factors are large for transitions in high-lying states of the ion. Nevertheless, radical cations are known to possess low-lying electronically excited states, and TDDFT calculations predict the first excited-state to lie 1.7 eV above the IP in the case of a vertical transition. We assume that the two bands (G2 and G3) in the TRPES originate from two ionization processes involving a different number of probe photons. Taking an adiabatic IP of 8.15 eV, a [1 + 3′] process corresponds to a maximum possible kinetic energy of 1.19 eV, and a [1 + 4′] process corresponds to 2.75 eV. A clear assignment of the two bands in the TRPES is not straightforward, and low-lying electronically excited states of the cation or intermediate resonances mediate the spectra. As apparent from the comparison of Figure 8 and Figure 16, the structure in the TRPES is linked to the multiphoton probe.

In contrast to the photoelectrons around 0.5 eV, the time-dependent signal at low kinetic energies is not well described by two time constants. If the relaxation proceeds via IC, the electronic energy will be converted to internal vibrational energy of the molecule and distributed in several vibrational modes. When ionizing the molecule in the probe step, this energy does not contribute to the kinetic energy of the photoelectrons. Under the assumption that the geometry of the species does not strongly change while relaxation to the a lower-lying state takes place, the time dependence of the low kinetic energy electrons can be explained. Taking the $IP_{vert} \approx 9.2$ eV of CPC into account,[28] ionization from the A $^1A''$ state (located at 1.54 eV in TD-B3P86/6-311^{++}G** calculations)[1] would produce a band of electrons around 0.08 eV when probing with five 795 nm photons (5 × 795 nm ≙ 7.79 eV). Thus ionization out of this state will produce electrons with low kinetic energy and suggests that observing these electrons (G3) is a possibility of ionizing the time dependence of the A $^1A''$ state. This picture can explain why the dynamics of the A $^1A''$ state becomes visible in the decay curve for G1, and the signal no longer decays to zero in the measured delay time. The signal will be weak since more probe photons are necessary to probe from lower lying electronic states. In a [1 + 3′] ionization, the primary populated 3 $^1A'$ state will also produce low kinetic energy electrons, since highly excited levels above the ionization limit can autoionize. Autoionization uses up some of the internal energy to overcome the ionization threshold and usually produces electrons with low kinetic energy.[44] The 795 nm multiphoton ionization, is likely to populate high-lying autoionizing states when probing the dense manifold of excited states illustrated in Figure 14. Therefore, all three time constants are visible in the photoelectron energy range of G1. Because the A $^1A''$ state is the lowest electronically exited state, the remaining time constants have to be linked to the dynamics of energetically higher lying states. Hence we assign the first decay constant $\tau_1 = 40$ fs of CPC to a relaxation within the dense manifold of initially excited states at around 4 eV. Subsequently, an IC with a time constant of 350 fs takes place into the A $^1A''$, converting the excess electronic energy into internal energy. Because of the existence of intermediate resonances, the ionization efficiency of the excited states between 3.67 and 4.01 eV will be much higher than the ionization efficiency of the A $^1A''$ with the 795 nm probe (1.56 eV). Thus the time-dependent ion signal in the lower trace of Figure 6 apparently decays to zero.

Excited State Dynamics of TFPC. Electronic spin resonance (ESR) indicates that TFPC has a triplet ground state[19] in contrast to CPC.[17] We computed the singlet state to be 17.4 kJ/mol higher in energy than the triplet state by DFT calculations. Thus the photophysics of the carbene will take place on the triplet potential energy surface. Interestingly both carbenes show similar dynamics in the time-resolved experiments, regardless of their ground-state spin multiplicity. TDDFT calculations on the excited states of triplet TFPC did not produce reliable results, because of the large number of electronic configurations contributing to each excited-state at the TD-B3P86/6-311^{+2}G** level of theory. Singlet TFPC gave a picture of the excited states similar to that for CPC when applying TDDFT. In order to acquire a more detailed explanation for the relaxation process of the triplet TFPC, higher level excited-state calculations by ab initio methods are necessary. Nevertheless, the data for TFPC indicate that the excited-state deactivation of TFPC follows a related mechanism to the deactivation of CPC. The initially prepared state decays within 60 fs, which is followed by a relaxation occurring within 500 fs. A third time constant on the order of several picoseconds was also extracted. The deactivation cascade again follows a "state I → state II → state III → ground state" scheme. Again the time dependence of electrons with low kinetic energy is different and indicates a third deactivation process.

Conclusions

TFPC and CPC can be cleanly generated by supersonic jet flash pyrolysis out of their corresponding diazirines. However, the isomerization barrier of MPC to styrene (only 31 J/mol) is not high enough to use the corresponding diazirine as a precursor for examination of MPC. The BMK functional is a cost-effective method for estimating whether side reactions in the pyrolysis source can take place or not.

We thus suggest the following model for the photochemistry of CPC: With short wavelength irradiation[9] an electron from the π-system of the aromatic ring is excited into the LUMO of the molecule.[1,18] This initially excited electronic state (3 $^1A'$) is presumably coupled to several other close-lying electronic states.

Our experiments conclude an ultrafast relaxation of around 40 fs within this dense manifold of the initially prepared state. Since the electronic states are energetically very close, the pump pulse will likely produce a wave packet composed of a superposition of electronic as well as vibrational states. The movement of the wave packet out of the FC region due to geometric deformations or a relaxation process between the close lying states explains the first 40 fs time constant. The remaining time constant of 350 fs has to be assigned to a subsequent relaxation to the A ^{1}A″ state.

From the present experiments, no information is available on how the A ^{1}A″ deactivates. Photoinduced isomerization at short wavelengths ($\lambda > 254$ nm) of CPC to CCHT has been reported in matrix experiments.[7] In principle, the photoreaction of CPC to CCHT could take place on the A ^{1}A″ state potential energy surface, and the third time constant corresponds to this process. However, because of the lack of diluents and the missing cage effect,[45] it is most likely that the C−Cl bond fission of CPC dominants over an isomerization to CCHT at isolated conditions after the primary photophysical relaxation processes have taken place. The loss of halides via predissociation has been observed for several isolated halocarbenes.[46] Since we do not observe any fragments of lower masses to grow in as a function of the time delay, and IC to the ground-state will be fast as a result of the many vibrational degrees of freedom of the molecule, we suggest that the third time constant represents the relaxation of the A ^{1}A″ state into the hot ground state. Any further reactions will thus take place on the hot ground-state surface.

In matrix experiments the large amount of excess energy deposited into the molecule by irradiation with $\lambda > 254$ nm enables isomerization to CCHT until the internal energy has been transferred to the diluents. Since CCHT is not reverted back to CPC at $\lambda > 254$ nm, all CCHT is preserved at matrix conditions. Further continuous irradiation of the matrix with $\lambda > 254$ nm will transfer all remaining CPC successively to CCHT.[9] Nevertheless, CCHT formation will only be of importance in condensed phase and most likely not in the isolated carbene.

The experiments on TFPC give evidence that the excited-state deactivation takes place in a very similar manner. This is rather surprising, considering that TFPC has a triplet ground state.

Acknowledgment. B.N. gratefully acknowledges a scholarship by the "Fonds der Chemischen Industrie", and R.M. acknowledges the SOLAMU grant by "Triangle de Physique". We thank Dominik Gehrig for helping to record the styrene spectrum. We thank the Deutsche Forschungsgemeinschaft (Fi 575/3-4), Laserlab Europe, and the DAAD, Egide (Procope), for financial support.

Supporting Information Available: Computational details on the TFPC singlet−triplet gap and DFT calculations on isomerization of MPC, mass spectra of 3,3-methylphenyldiazirine, and the full citation for ref 35. This material is available free of charge via the Internet at http://pubs.acs.org.

References and Notes

(1) Noller, B.; Poisson, L.; Maksimenka, R.; Fischer, I.; Mestdagh, J.-M. *J. Am. Chem. Soc.* **2008**, *130*, 14908.
(2) Noller, B.; Maksimenka, R.; Fischer, I.; Armone, M.; Engels, B.; Alcaraz, C.; Poisson, L.; Mestdagh, J.-M. *J. Phys. Chem. A* **2007**, *111*, 1771.
(3) Zierhut, M.; Noller, B.; Schultz, T.; Fischer, I. *J. Chem. Phys.* **2005**, *122*, 094302.
(4) Bettinger, H. F.; Schreiner, P. R.; Schleyer, P.; Allinger, N. L.; Clark, T.; Gasteiger, J.; Kollman, P.; Schaefer, H. F. *Encyclopedia of Computational Chemistry*; John Wiley & Sons: Chichester, 1998.
(5) Baron, W. J.; Decamp, M. R. *Tetrahedron Lett.* **1973**, *17*, 4225.
(6) Geise, C. M.; Hadad, C. M. *J. Org. Chem.* **2002**, *67*, 2532.
(7) Sander, W.; Bucher, G.; Wierlacher, S. *Chem. Rev.* **1993**, *93*, 1583.
(8) McMahon, R. J.; Abelt, C. J.; Chapman, O. L.; Johnson, J. W.; Kreil, C. L.; Leroux, J. P.; Mooring, A. M.; West, P. R. *J. Am. Chem. Soc.* **1987**, *109*, 2456.
(9) Sander, W. W. *Spectrochim. Acta* **1987**, *43A*, 637.
(10) Wang, J.; Burdzinski, G.; Kubicki, J.; Platz, M. S.; Moss, R. A.; Fu, X. L.; Piotrowiak, P.; Myahkostupov, M. *J. Am. Chem. Soc.* **2006**, *128*, 16446.
(11) Stolow, A. *Annu. Rev. Phys. Chem.* **2003**, *54*, 89.
(12) Moss, R. A. *Acc. Chem. Res.* **2006**, *39*, 267.
(13) Blencowe, A.; Hayes, W. *Soft Matter* **2005**, *1*, 178.
(14) Kohn, D. W.; Clauberg, H.; Chen, P. *Rev. Sci. Instrum.* **1992**, *63*, 4003.
(15) Whitaker, B. *Imaging in Molecular Dynamics*; Cambridge University Press: Cambridge, 2003.
(16) Gross, C.; Noller, B.; Fischer, I. *Phys. Chem. Chem. Phys.* **2008**, *10*, 5196.
(17) Gould, I. R.; Turro, N. J.; Butcher, J.; Doubleday, C.; Hacker, N. P.; Lehr, G. F.; Moss, R. A.; Cox, D. P.; Guo, W.; Munjal, R. C.; Perez, L. A.; Fedorynski, M. *Tetrahedron* **1985**, *41*, 1587.
(18) Pliego, J. R.; De Almeida, W. B.; Celebi, S.; Zhu, Z.; Platz, M. S. *J. Phys. Chem. A* **1999**, *103*, 7481.
(19) Wasserman, E. *J. Chem. Phys.* **1965**, *42*, 3739.
(20) Graham, W. H. *J. Am. Chem. Soc.* **1965**, *87*, 4396.
(21) Brunner, J.; Senn, H.; Richards, F. M. *J. Biol. Chem.* **1980**, *255*, 3313.
(22) Liu, M. T. H.; Ramakrishnan, K. *J. Org. Chem.* **1977**, *42*, 3450.
(23) Garcia, G. A.; Nahon, L.; Powis, I. *Rev. Sci. Instrum.* **2004**, *75*, 4989.
(24) Kuthirummal, N.; Weber, P. M. *Chem. Phys. Lett.* **2003**, *378*, 647.
(25) Song, J.-K.; Tsubouchi, M.; Suzuki, T. *J. Chem. Phys.* **2001**, *115*, 8810.
(26) Tsubouchi, M. S.; Suzuki, T. *J. Phys. Chem. A* **2003**, *107*, 10897.
(27) Zierhut, M.; Roth, W.; Fischer, I. *J. Phys. Chem. A* **2004**, *108*, 8125.
(28) Noller, B.; Hemberger, P.; Fischer, I.; Alcaraz, C.; Garcia, G.; Soldi-Lose, H. submitted to *Phys. Chem. Chem. Phys.* 2009.
(29) Nassal, M. *Liebigs Ann. Chem.* **1983**, 1510.
(30) Syage, J. A.; Al Adel, F.; Zewail, A. H. *Chem. Phys. Lett.* **1983**, *103*, 15.
(31) McMahon, R. J.; Chapman, O. L. *J. Am. Chem. Soc.* **1987**, *109*, 683.
(32) Pederson, S.; Zewail, A. H. *Mol. Phys.* **1996**, *89*, 1455.
(33) Bettinger, H. F.; Schleyer, P. V.; Schaefer, H. F.; Schreiner, P. R.; Kaiser, R. I.; Lee, Y. T. *J. Chem. Phys.* **2000**, *113*, 4250.
(34) Boese, A. D.; Martin, J. M. L. *J. Chem. Phys.* **2004**, *121*, 3405.
(35) Frisch, M. J.; Trucks, G. W.; Schlegel, H. B. *Gaussian 03, Revision C.02*, 2004.
(36) Rosenberg, M. G.; Brinker, U. H. *J. Org. Chem.* **2003**, *68*, 4819.
(37) Peng, C.; Ayala, P. Y.; Schlegel, H. B.; Frisch, M. J. *J. Comput. Chem.* **1996**, *17*, 49.
(38) Chung, G.; Lee, D. *Chem. Phys. Lett.* **2001**, *350*, 339.
(39) Worthington, S. H.; Cramer, C. J. *J. Phys. Org. Chem.* **1997**, *10*, 755.
(40) Garcia, V. M.; Castell, O.; Reguero, M.; Caballol, R. *Mol. Phys.* **1996**, *87*, 1395.
(41) Cramer, C. J.; Truhlar, D. G.; Falvey, D. E. *J. Am. Chem. Soc.* **1997**, *119*, 12338.
(42) Gasser, M.; Bach, A.; Chen, P. *Phys. Chem. Chem. Phys.* **2008**, *10*, 1133.
(43) West, P. R.; Chapman, O. L.; LeRoux, J. P. *J. Am. Chem. Soc.* **1982**, *104*, 1779.
(44) Raptis, C. A.; Pratt, S. T. *Phys. Rev. Lett.* **2000**, *84*, 5078.
(45) Poisson, L.; Roubin, P.; Coussan, S.; Soep, B.; Mestdagh, J.-M. *J. Am. Chem. Soc.* **2008**, *130*, 2974.
(46) Tao, C.; Reid, S. A.; Schmidt, T. W.; Kable, S. H. *J. Chem. Phys.* **2007**, *126*, 051105.

JP810974M